Single-Laser Optical Tweezers

Background, Applications, and Calibration Methods

Matheus Macena de Carvalho

Advised by:
Dr. Bjorg Larson
Dr. James Supplee
Dr. Brianne Barker

Specialized Honors Thesis
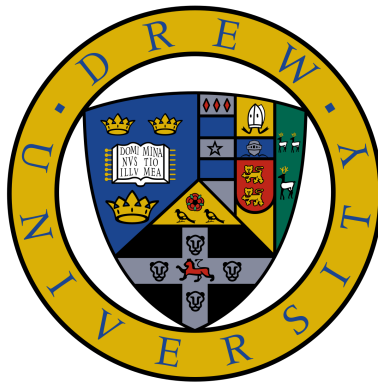
Department of Physics
Drew University
May 2021

Abstract

Through the studies of radiation pressure and using recently developed laser technologies, optical tweezers were invented by Dr. Arthur Ashkin. Recent biological and quantum physics applications motivated the study of optical trapping systems at Drew University. During Drew Summer Science Institute in 2019, 1 micron polystyrene beads were recorded trapped and manipulated on the sample plane of a custom-made optical tweezers setup. The bulk of the setup was then replaced by a Zeiss Axioplan 2 microscope to attempt measuring the trapping stiffness applied on the beads. Multiple calibration methods are addressed and the feasibility of their implementation is discussed. Both theoretical, Rayleigh Regime, and experimental calibration methods, Brownian Harmonic Oscillator, are used to quantitatively determine the trapping stiffness of a system. Although the Rayleigh Regime makes an approximation for beads not in this study's range, it serves as a basis of comparison to the experimental data. Through the use of a quadrant photodiode, the Brownian Harmonic Oscillator method analyzes the thermal fluctuations of a trapped bead. These fluctuations are converted into frequencies, which are linearly proportional to the trapping stiffness. The theoretical, and experimental calibration methods yield similar results, in the same order of magnitude, and increase the trapping stiffness with greater laser power. Future applications to increase the reliability of the system calibration, such as the calibration of the quadrant photodiode, parameters variations, and new calibration methods are then addressed.

Acknowledgements

Contents

List of Figures and Tables

Chapter 1

Introduction

This chapter will introduce the main physical forces related to optical tweezers: radiation pressure, gradient, and scattering forces, while presenting their effects on the trapping object. Also, it will present the history of optical tweezers, referring to interviews, statements, and papers from Dr. Arthur Ashkin, and Dr. Steve Chu, its creators. Then, the development of optical tweezers and its relevance in current applications will be discussed. A special passage on honor of the Nobel Prize in Physics awarded by Arthur Ashkin "for the optical tweezers and their application to biological systems" will also be addressed.

This introduction will also discuss the physics behind optical tweezers. It will describe how a particle is trapped from its simplest conceptual interpretation to the Rayleigh regime solution, which is an absolute calibration method for Rayleigh particles, which compares trapped objects with dipoles.

Ultimately, the state of Optical Tweezers at Drew University will be considered. The addition of optical trapping systems research in Dr. Larson's optics lab in the 2019 Drew Summer Science Institute, as well as the current status of this research project and the new implementations, and calibration methods that were applied to the system.

1.1 Historical Background

1.1.1 Radiation Pressure

Radiation pressure is the foundation of optical trapping technologies. It has been studied since 1619, when Johannes Kepler indicated the phenomenon of comets' tails always pointing away from the sun. Since then, the idea of light pushing onto objects and exerting pressure onto surfaces was put forward to the public, and studied by many scientists. Much later, in 1862, James Clerk Maxwell described light as a propagating wave of electric and magnetic fields, which consequently should follow the same patterns predicted by his well known equations (Maxwell's equations).

The assertion that light, as an electromagnetic wave, imparts momentum in solid bodies was first proven experimentally by Pyotr Lebedev in 1900. His studies were confirmed by Ernest Fox Nichols and Gordon Ferrie Hull in 1901, who made use of the Nichols radiometer. It consisted of a pair of mirrors suspended as a torsion balance, within a chamber with controlled air pressure. A beam of light was pointed at the first mirror, reflected onto the second, and the deflections due to radiation

pressure were measured by the projections of the reflected light beam. With low air pressure, the Nichols Radiometer was able to predict the displacement of mirrors with 99% of accuracy.

Radiation pressure, nonetheless, is much more evident in the wider scale, and it plays a major role in multiple cosmic effects. For example, it works as a counterforce pushing against the material in massive stars, resisting it to collapse in on itself. Radiation pressure also supports the Big Bang theory during a phase called the photon epoch. It dominated the energy of the universe from 10 seconds after the Big Bang, until the temperature was low enough for nuclei to combine with electrons to create neutral atoms, more than 300,000 years later.

After the 1900's, radiation pressure made its appearance on the smaller scale. It is support for quantum optics, biomicroscopy, optomechanics, and optogenetics. It can be described in terms of quantum and even classical mechanical theories, as it can be illustrated by Newton's Third Law. Any change in the momentum of light, in either its wave or photon state, will result in a change of the momentum of the media, or any surface that it interacts with.

1.1.2   History of Optical Tweezers

Dr. Arthur Ashkin, working at Bell Labs, had this dream: "Wouldn't it be nice if you can hold on to an atom with light?" [7]. Ashkin focused his research in light pressure, and light levitation projects, which solidified his persistence in building optical tweezers (term created by Ashkin himself).

In 1970, Ashkin first detected optical scattering and gradient forces, the key forces for optical trapping, on micron sized transparent particles. However, the project did not get much progress over the following 10 years. There was no evidence that Dr. Ashkin was "holding onto" particles with light, so his superiors cut his funding, and he was asked to move on to other projects. Dr. Ashkin continued to pursue his dream anyway, and in 1983 he enlisted Dr. Steven Chu to join his research project, who had recently joined the Holmdel, New Jersey branch of Bell Labs.

During a snowstorm, Dr. Chu considered cooling an atom before the attempt of trapping it, the reverse process of what had been attempted previously. "What if you cooled down the atom first? Don't hold onto it, but maybe in the process of cooling it down, it's going to hang around for enough time that you can have a chance of grabbing onto it." [7]. Atom trapping would require means to slow atoms down to a kinetic energy less than the energy generated by the trapping light. Based on Einstein's model of Brownian motion, Dr. Chu lowered the temperature of the atom, and therefore the average speed of its random walks. Reducing the thermal energy of the atom made it easier to push the atom around (or trap it) with very weak forces.

In 1986, Ashkin, Dziedzic, Bjorkholm, and Chu published the first scientific article confirming the existence of "negative radiation pressure". This negative radiation pressure can be explained by a stronger gradient force, due to the change in pressure, than the scattering force, due to the reflection and absorption of light onto a particle. This experiment showed the possibility of trapping particles regardless of their size, from Rayleigh particles (much smaller than the laser wavelength) to Mie particles (much larger than the laser's wavelength).

1.1.3   Development of Optical Tweezers and Applications

As optical tweezers allow trapping and manipulation of micron and nano particles, there are multiple research projects taking advantage of these features. Trapping dielectric spheres, viruses, bacteria, living cells, organelles, small metal particles, and even strands of DNA has developed new ways of measuring forces and studying motions that have never been examined before.

Many applications emerge from or make use of optical tweezers, including: cell sorting [20], tracking bacterial motility and motion patterns [22] [15], nanotechnologies [23], optical binding [21], single-molecule force spectroscopy [13], studying physics concepts such as the Casimir effect [26], Stochastic thermodynamics [24], and in the field of quantum mechanics, such as the Bose-Einstein condensate state [18] and quantum gravity [29].

For single-molecule or other nanoscale trapping projects, dielectric spheres are chemically attached to the specimen. As the theory for optical tweezers forces on dielectric spheres have been further developed, the specimen, after trapped, can be analyzed and studied through separate imaging systems. Optical tweezers have also been a great development in the study of inter and intra-molecular forces.

On the theoretical perspective, much effort has been put into developing feasible calibration methods. These methods must agree with the theory behind the relationship between light and matter and be able to interpret the forces observed in experiments. However, most of these theoretical methods require complex analyses and certain parameters, such as detector sensitivities, which are not known to a sufficient precision and experimental calibrations are often preferred. The most accepted theory for particles in the size range of proteins and bacteria in a optical trapping device is the Lorentz-Mie Scattering Theory. This theory is an exact analytical solution of Maxwell's equations, which although mentioned, is beyond the scope of this research.

This thesis will cover multiple theoretical and experimental calibration methods. It will use a general description of the Rayleigh particle regime to predict the trap stiffness of this current setup. Also, it will compare the theoretical data with an experimental method, the Brownian Harmonic Oscillator, using a quadrant photodiode as a position sensing detector. Finally, it will analyze the data and predict the trapping stiffness of the current optical trapping system at Drew University.

1.1.4   2018 Nobel Prize in Physics

In 2018, the Royal Swedish Academy of Sciences awarded the Nobel Prize in Physics to Dr. Arthur Ashkin, "for the optical tweezers and their application to biological systems." His Nobel Lecture was held by René-Jean Essiambre at the Aula Magna, Stockholm University. He was introduced by Professor Olga Botner, Chair of the Nobel Committee for Physics. Ashkin, at the time, was the oldest Nobel Prize winner in 2018, at 96 years old. In 2019 John B. Goodenough, at 97, won the Nobel Prize in chemistry.

Ashkin shared half of the prize with Donna Strickland, and Gerard Mourou "for their method of generating high-intensity ultra-short optical pulses" [27]. Strickland won the prize for the work she did as a PhD student, and Mourou was her supervisor. She became the third woman to ever win a Nobel Prize in Physics.

1.2   Physics Behind Optical Tweezers

1.2.1   Optical Trapping Forces

Optical trapping forces arise from the interaction between light and matter, or radiation pressure. The pressure-gradient force can overcome the scattering force of the light reflection and produce a "negative radiation pressure" [1], forcing a particle to move towards the focal point. A single laser beam focused by a high numerical aperture (NA) objective lens is able to trap dielectric particles near its focal point, due to its gradient force. A high NA represent a small focal point and therefore, a small beam waist. The beam waist is the width of the beam at the narrowest point of the focused beam. As $P = F/A$, a smaller beam waist indicates a bigger pressure, and a higher gradient force.

However, light and matter interactions behave differently for various scales. The simplest approach and more intuitive explanation for the trapping force applies in objects with radii much greater than the light's wavelength. The trapping force can be explained by conservation of momentum, and the refraction of the light in the trapped object due to its greater refractive index than the media.

The refraction of the rays is described by the Snell's Law:

$$n_1 \sin\theta_1 = n_2 \sin\theta_2, \tag{1.1}$$

where n_1 and θ_1 are, respectfully, the index of refraction and the angle of incidence of the origin's media, and n_2 and θ_2 of the consequent media. Note that, in an optical tweezers setup, Snell's law comes up multiple times. However, the most relevant instance is when the rays go from the viscous media into and out of the trapped particle. The trapped particles are most commonly spheres, which facilitates the projections of the refracted rays. As seen in figure 1.1 there is a change of momentum of light, due to the change in the direction of its rays. By conservation of momentum, the trapped object experiences a force contrary to the net force of all refracted rays, which is towards the objective lens' focal point.
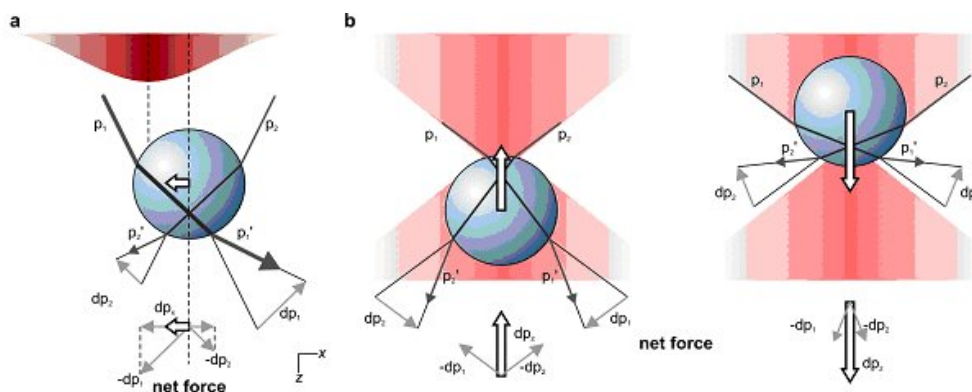
Figure 1.1: Change in momentum of light refracted in a trapped bead from [12]. Note that the light gets darker in the center and fainter towards the extremes to indicate the power distribution in a Gaussian beam

In figure 1.1a, the trapped object is off-center perpendicularly to the beam's axis. As the incident light has a Gaussian distribution, the rays towards the center have greater power, which are indicated in the picture by p_1 being larger and thicker than

p_2. As the net momentum of the refracted rays is towards the right, the trapped object experiences a net force towards the left, and towards the laser's focus. These two rays in figure 1.1a represent the global effect of all rays, coming from the central portion and from the right hand portion of the Gaussian intensity profile. Similarly, off-center displacements in the direction of incident beam cause net forces in the opposite direction, as in figure 1.1b. It is clear that the resulting force always points towards the objective's focal point for any position of the trapped object relative to the center of the beam. This force can be considered a "restoring force" that always pushes the particle back to the center.

As mentioned previously, this method is only valid for Mie particles, objects with much greater size than the incident lights' wavelength. Also, it does not take into account some factors, such as the absorption and reflection of the incident rays. The magnitude of the trapping force on the particle will be covered later in this paper and depends on many factors, such as: the power (P) and wavelength (λ) of the light source, the numerical aperture (NA) of the objective lens, the refractive index of the media (n_m) and of the particle (n_p), and the diameter (D) and mass (m) of the trapped particle.

Many researchers have been trying to develop theories to quantitatively describe the optical trapping forces. The Generalized Lorentz-Mie Scattering Solution is an exact analytical solution of Maxwell's equation for the scattering light by spherical particles. This theory can be used for Mie particles and it has also been adapted to Rayleigh approximation, with particles much smaller than the wavelength of the trapping light source. The theoretical and experimental calibration methods used for this project will take into account the size of the trapped polystyrene beads, which are 1μm in diameter, and therefore in the size range of the laser beam's wavelength (488nm). However, the complexity of the exact solutions for this particle size range required adaptations on the calibration methods selected.

1.2.2   Spherical Aberrations

Spherical aberrations from the focusing lens cause a reduction in the trapping efficiency. Spherical lenses are much more accessible and easier to fabricate than aspherical lenses. However, its spherical shape causes peripheral rays to bend either more (positive spherical aberration) or less than rays at the center of the lens (negative spherical aberration).

Figure 1.2 represents the spherical aberrations influence in the efficiency of a tweezers setup. Due to the spherical shape of the lenses in the objective lens, most of the setups experience this effect. The external rays are bent more than necessary, which causes them to have an earlier focal point than the internal ones, generating positive spherical aberrations (most commonly). Therefore, the focal point gets expanded into a focal region, increasing the trapping area and decreasing the gradient force of the system.

(a) Focal point of an oil objective lens ignoring Spherical Aberrations

(b) Focal region of an oil objective lens taking into account Spherical Aberrations
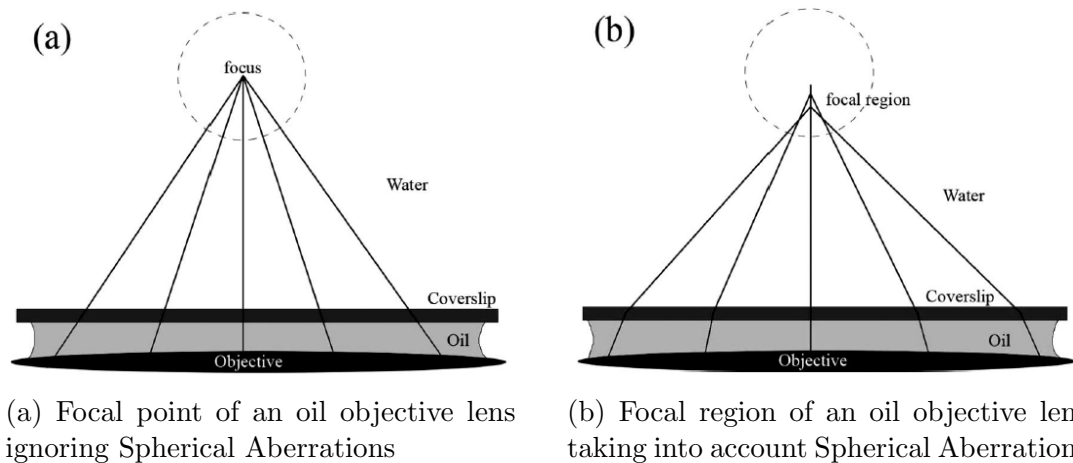
Figure 1.2: Evidence of Spherical Aberrations due to refraction in the objective lens from [16]

1.3   Optical Tweezers at Drew University

1.3.1   2019 Drew Summer Science Institute

In the 2019 Drew Summer Science Institute (DSSI), Aidan Carter, Gabriel Mohideen, and Matheus Macena de Carvalho joined Dr. Larson's optics lab to work on her Line-Scanning Confocal Microscopy project. The project had the ultimate motivation of developing a feasible system to view cell structure beneath skin without cutting any tissue. There exists point-scanning confocal systems which can analyze cell structure in different depths of skin with great resolutions, however the systems are too big and bulky, and are not feasible for clinical use. Line-scanning microscopes are simpler and they can be made more compact for clinical use however, they have less resolution than point-scanning as they use a slit instead of a pinhole to block out-of-focus light into the detector, making the images hazy and blurry.

The goal for the 2019 DSSI project was to increase the sectioning capability, and therefore improving the resolution of our system. In order to do so, a background subtraction data processing technique was introduced to the system, which records the focused and out-of-focus light from the detector, then subtracts the out-of-focus light to eliminate the haziness from the final data. A single point detector was used to determine our alignment ability and our improvement on the sectioning capability and resolution of our system with the subtraction technique, which showed great results.

However, previous to the use of the subtraction technique with an imaging camera, an accident forced the group to completely change the expected pathways for the next few weeks of research. The service board of our camera was burned. The board was a unique, custom made piece of equipment, which controlled the frame rate of the system. So, as Dr. Larson's lab had high-power lasers and objective lens with high numerical aperture, the group decided to build an optical tweezers. The decision for the project was based on the recent surge on the applications for optical tweezers and took into consideration that it recently won the Nobel Prize in Physics in 2018.

Most of the components needed for a simple optical tweezers setup were gathered,

and the development of the Drew Physics's setup had started. One of the missing components was a mirror to reflect the laser beam onto the objective lens while not blocking the light source for the camera. After analyzing multiple simple optical tweezers setups and papers, there was two possible options for this issue: using a polarizing beamsplitter and a quarter-wave plate to change the polarization of the laser to circularly polarized, and reflecting 50% of the light to the objective and transmit the other 50%; or using a dichroic mirror, which would reflect only a small range of wavelengths and transmit all other wavelengths, reflecting the laser and letting through the light source for the camera.

As there was a quarter-wave plate available in the department, a polarizing beamsplitter cube was purchased. However, some days later, going through boxes of optics components that were donated to the Drew Physics department, a dichroic mirror that reflected more than 90% of the laser source was found. The dichroic mirror was bigger and easier to implement to the system than the polarizing cube, which is still unused, but could be implemented in many other experiments.

The setup was composed of a 408nm 120mW violet laser and multiple other optics components. An illustration and detailed explanation of the components can be found in figure 1.3, and table 1.4.
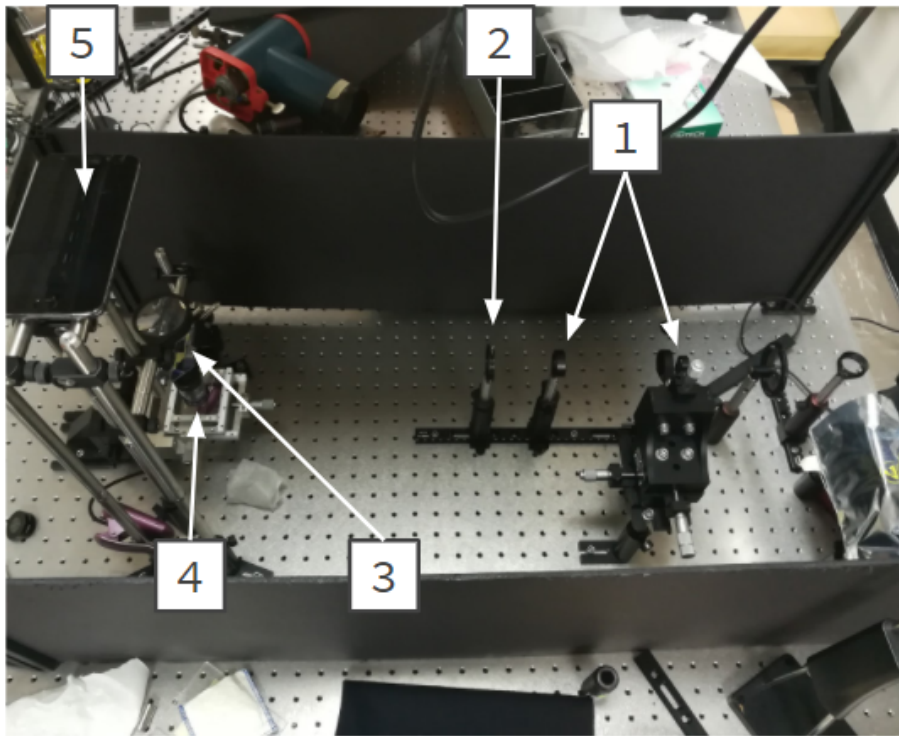
Figure 1.3: Picture of 2019 DSSI Optical Tweezers Setup

At the end of DSSI, videos were recorded to demonstrate the trapping and manipulation of 1-micron polystyrene beads. As the dichroic mirror was mounted in a very fine kinematic mount, beads were dragged onto the sample plane by slightly moving the dichroic mirror. That process misaligns the system lightly, as the laser beam would shift away from the center of the objective's rear aperture, changing the trapping force as well. In order to fix this issue, the sample stage should be moved instead of the dichroic mirror. However the stage did not have as fine control as the dichroic's mount and any movement in the stage would shake the whole sample

Components	Function
1: Beam Expander	The beam expander is composed by two converging lens of focal lengths 13mm and 125mm, expanding the beam nearly 10 times.
2: Pinhole and Iris	In between the beam expander there is a pinhole serving as a spatial filter. Also, at the end of the second lens, there is an iris decreasing the divergence of light hitting the dichroic mirror.
3: Dichroic Mirror	Yellow dichroic mirror, which reflects wavelengths (laser used has 408nm in wavelength) and let through all other wavelengths (most of white light source used for the camera).
4: Sample Stage and Objective Lens	2D sample stage used to mount slide with sample and cover slip. 60x magnification oil objective lens (1.42 NA)
5: Mounted support for the camera	Support contained two lenses in order to magnify the image of illuminated sample, with the laser light filtered out by the dichroic and the camera (smartphone).

Table 1.4: Components in the 2019 DSSI Optical Tweezers Setup

and release the bead away from objective's focal region. Although trapping and manipulation of the beads were demonstrated, there was no time left in DSSI for the group to dive into calibrating, and investigating the trapping stiffness of the system.

1.3.2   2020 Specialized Honors Thesis

When deciding to pursue a senior honors thesis, immediate thoughts were onto the optical tweezers system that was recently built and reserved plenty of room for development. The Drew Physics Department had also recently received a donation of a Zeiss Axioplan 2 microscope, so the first plan was to integrate the microscope into the 2019 DSSI Setup. The microscope was a foreign piece of equipment to the research members, so some time was necessary to become familiar with all of its functionalities. Details of the implementation of the microscope and of the current layout for the system can be found in the following chapter.

Chapter 2

Methods

This chapter will thoroughly discuss the design, functionality, and the new implementations of the optical tweezers setup. It will also discuss multiple calibration methods: two theoretical approaches, for particles with diameter much smaller and much greater than the incident light's wavelength; and an experimental approach, the Brownian Harmonic Oscillator Method, comparing the trapped particle with the elastic behavior of a spring. Rayleigh particles regime and Brownian harmonic oscillator have been used to calibrate the optical tweezers trapping stiffness.

2.1   New System's Design

2.1.1   Implementing the Zeiss Microscope

The alignment routine and the fragility of the previous setup encouraged the implementation of a Zeiss microscope that was donated to the Drew Physics Department. The microscope is a useful piece of equipment, with multiple dichroic beamsplitters, filters, and objective lenses available. The most powerful objective lens (Zeiss Plan-APOCHROMAT 63x/1.40 OIL DIC) was chosen to focus the incident laser beam (Coherent Sapphire 488 LP, 100 mW).

Previous to the assembly of the new optical tweezers set up, some time was necessary to become familiar with the Zeiss Microscope. As the microscope was not previously used for optical trapping, multiple components had to be removed or replaced as they altered or fully blocked the laser path, as illustrated in figure 2.1.

The implementation of the microscope, although complicated, offered pros and cons relative to a custom made system as the one built in 2019. A more thorough analysis of this transition can be found in the discussion section. The current setup is a major improvement from the previous alignment system, which was fragile and needed to be re-aligned almost daily. The DSSI setup required alignment of each individual component: beamsplitter, dichroic mirror, objective lens, tube lens, and eyepiece. In the other hand, the Zeiss microscope has all those components aligned into the same device.

The setup for the new system is very similar to the DSSI setup, however instead of having one dichroic mirror mounted, there are eight numbered dichroic beamsplitters available in the Zeiss microscope. Table 2.2 shows the power of the 488nm laser through each beamsplitter available, and the percentage of the transmitted power (not reflected or absorbed by the beamsplitters).

(a) Beam blocker fixed at the back entrance of the Zeiss Microscope, which absorbed all of the laser light.

(b) Dimmer located after the condenser lens to reduce the intensity of the incident laser. The dimmer was removed to increase the space available after the condenser to implement the QPD.

(c) Mirror at the back entrance of the Zeiss Microscope, which could be moved in and out of the laser path.

Figure 2.1: Elements removed from Zeiss Microscope. Note that there were several other similar elements, which were removed as they blocked or altered the path or intensity of the laser beam.

2.1.2 Layout of the System

Figure 2.3 and table 2.4 illustrate and give a brief explanation of the optical components used in the new set up. Note that the Quadrant Photodiode (QPD) was implemented later on, and is not included in this section. The QPD is not required for the trapping and it is used solely to capture data from the trapped object. More information on the implementation and use of the QPD can be found in the following sections.

According to the numbers in figure 2.3 and table 2.4, the layout of the system can be described as: the laser (1) is redirected with flat mirrors through the iris (2); it passes through a filter (3) to adjust the intensity of the beam; goes through a beam expander (4), which consists of two converging lenses, with 13 mm and 125 mm of focal lengths respectfully to expand the beam to a size compatible with the objective lens' aperture; goes though the back entrance of the Zeiss Microscope; gets reflected by a selected dichroic beamsplitter (8) onto the objective lens (9), which focus the laser onto a point in the sample stage (10); the laser light with data from the sample goes through condenser (11), which increases the light coherence to be reflected onto the QPD, which will analyze the data; the white light source (12) illuminates the sample plan for its visibility at the eyepiece (7) and the camera port (8).

Beamsplitter #	Laser Power Transmitted (mW)	Percentage Transmitted (%)
1	49.1	54.5
2	0	0.0
3	0	0.0
4	0	0.0
5	60.7	67.4
6	0	0.0
7	36.5	40.5
8	45.4	50.4

Table 2.2: Laser Power through each beamsplitter from the Zeiss Microscope. Note that 4 beamsplitters (#2, #3, #4, and #6) block, or reflect, all of the 488 nm laser, and #5 was the chosen beamsplitter as it is the best transmitter for the laser's wavelength.
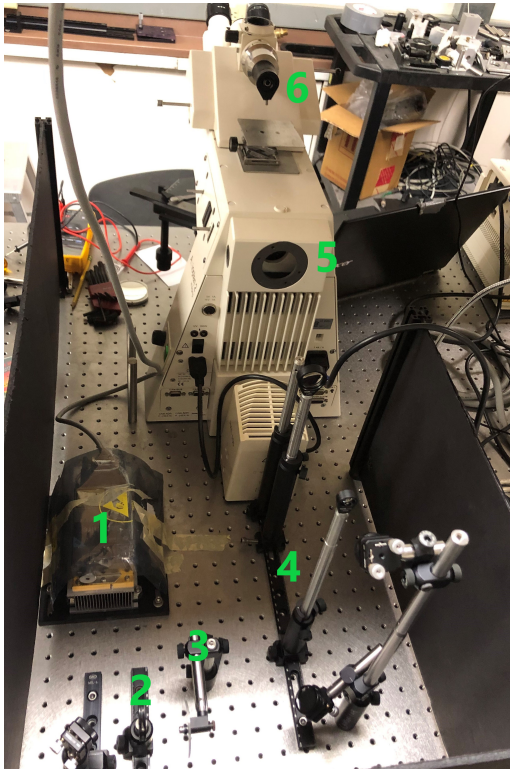
(a) Back of the Zeiss Microscope and arrangement of the optical components directing the incident laser beam to the back entrance of the microscope.
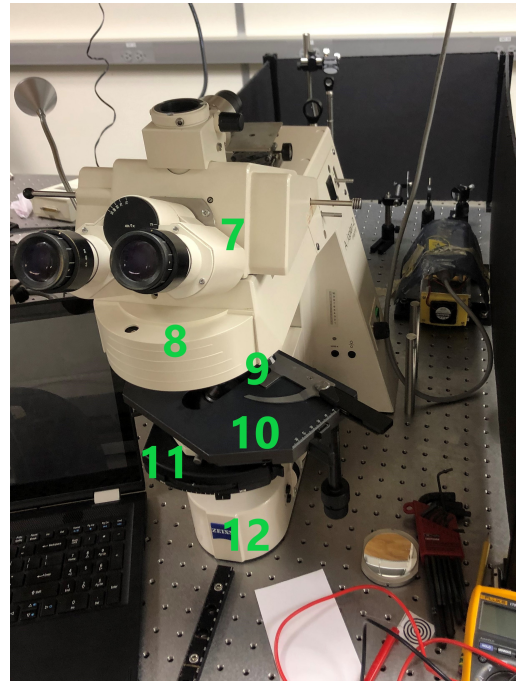
(b) Front of the Zeiss Microscope. Note that underneath the eyepiece there is a semi cylinder which contains 8 dichroic beamsplitters that reflect the laser light to the object lenses (right above the stage). The beamsplitters also reflect the white light from underneath the stage into the eyepiece and camera ports on the top part of the microscope.

Figure 2.3: Layout of the new optical tweezers set up. Note that a more thorough explanation of the components can be found in table 2.4.

2.2 Calibration Methods

The transfer in momentum between electromagnetic waves and particles can be demonstrated by Maxwell's theory and the resultant force of a single ray can be

Components	Description
1: 100mW 488nm Laser	Trapping Light Source
2: Iris	Block scattered light from first mirror
3: Filter	Filter laser beam to desired intensity
4:Beam Expander	Expands the laser beam to fulfill objective lens aperture
5: Microscope Back Entrance	Focus the laser beam onto beamsplitter and sample
6: Camera Port	Port and custom stage for camera to view sample
7: Eyepiece	Pair of Zeiss Microscope Eyepieces
8: Dichroic Beamsplitters	Container with 8 dichroic beamsplitters
9: Objective Lens	Focus the laser beam onto the sample
10: Stage	Position the sample slide onto the laser focus
11: Condenser	Focus the laser light to a more coherent beam
12: White Light Source	Illuminates the sample to be viewed through camera port or eyepiece

<div align="center">Table 2.4: Table of components of the new optical tweezers system</div>

illustrated by:

$$F \alpha \frac{P_r}{v}, \tag{2.1}$$

where F is the force of a single ray with power P_r and velocity v. The velocity of the ray is dependent on the refractive index of the medium n_m by:

$$v = \frac{c}{n_m}. \tag{2.2}$$

The change in momentum exerted by a photon can be described by considering a light beam incident perpendicular on a plane mirror. Each photon has momentum $\hbar \vec{k}$, where $\vec{k}$ is the wave vector. After reflection, the momentum of this photon is -$\hbar \vec{k}$, therefore the momentum transferred to the mirror is

$$\Delta \vec{p} = 2\hbar \vec{k}. \tag{2.3}$$

The magnitude of the change in momentum can be written as:

$$\Delta p = 2\hbar k = 2\frac{\hbar \omega}{v} = 2\frac{E}{v}, \tag{2.4}$$

where E is the photon energy and ω is the angular frequency. As the force can be written as the first derivative of momentum in respect of time, as:

$$F = \frac{dp}{dt} = \frac{2}{v}\frac{dE_{beam}}{dt} = 2\frac{P_{beam}}{v}. \tag{2.5}$$

In this project, the laser used has 100 mW in power, which is decreased before reaching the sample due reflection and absorption in other optical components. As a filter is used to adjust the desired power of the beam, the power intensity at the sample can range from 0.1 mW to 40 mW. Also, the sample medium for this system

is distilled water, which has an refractive index of 1.333. Using equation 2.5, the force is predicted to be of the order piconewtons ($1pn = 10^{-12}N$).

This force would not be able to describe an optical tweezers trapping force as it pushes the mirror (object) in the direction of the incident light. As discussed in chapter 1, all objects can refract and reflect multiple photons. Trapping can only be observed when the gradient force, due to the refraction of light as in figure 1.1 is greater than the scattering force, due to reflected photons. This only occurs when a powerful laser beam is tightly focused by a high numerical aperture objective lens.

2.2.1   Theoretical Calibration Methods

Rayleigh Particles Regime

This solution is only valid when the beam phase shift is small when refracted at the bead, or

$$2ka(m - 1) \ll 1, \tag{2.6}$$

where k is the wave vector, which could be simplified by $k = 2\pi n_m/\lambda$, a is the bead radius, λ is the wavelength of the incident laser beam, and m is the relative refractive index ($m = n_b/n_m$), where n_b and n_m are the refractive index of the bead and the medium, respectively. In most systems where $m > 1$, which includes this optical tweezers setup, equation 2.6 can be as simple as $a \ll \lambda$.

Due to its size, the Rayleigh approximation treats the dielectric sphere, or bead, as a volume of dipoles in an approximately uniform electric field, the incident laser beam, as found in [4] and [6]. The electric potential energy formula for a dipole can be written as:

$$U = -\vec{p} \cdot \vec{E}, \tag{2.7}$$

and the force on the dipole can be found by the gradient of this potential energy:

$$\vec{F} = -\vec{\nabla}U = \vec{\nabla}(\vec{p} \cdot \vec{E}). \tag{2.8}$$

The force acting on the bead can be found by the induced dipole moment of the dielectric sphere **p**, which is:

$$\vec{p}_{grad} = 4\pi\epsilon_0 \frac{m^2 - 1}{m^2 + 2} a^3 \vec{E}, \tag{2.9}$$

where $\vec{E}$ is the electric field outside the trapped object.

Using equations 2.8 and 2.9 the gradient force acting on the trapped bead is

$$\vec{F}_{grad} = 4\pi\epsilon_0 \frac{m^2 - 1}{m^2 + 2} a^3 \vec{\nabla} E^2. \tag{2.10}$$

The intensity of the beam (I) is directly proportional to the square of its electric field as

$$I = \frac{1}{2}c\epsilon_0 E^2. \tag{2.11}$$

Therefore, the time-averaged gradient force can be written as:

$$\vec{F}_{grad} = \frac{2\pi n_m}{c} a^3 \left(\frac{m^2 - 1}{m^2 + 2} \right) \vec{\nabla} I(\vec{r}). \tag{2.12}$$

The gradient force acts perpendicularly, or even opposite, to the direction of the incident beam, which explains the "negative" radiation force term. Equation 2.10 shows that the force acting on a trapped object is proportional to the gradient of the electric field, and therefore of the intensity of the incident beam. The gradient force points towards the region with maximum beam intensity (focal region).

While, the scattering force, due to the absorption and re-radiation of light by the dipole, can be written as [9]:

$$\vec{F}_{scat} = \frac{128\pi^5 a^6 n_m}{3c\lambda^4} \left(\frac{m^2-1}{m^2+2}\right)^2 I(\vec{r})\vec{z}. \tag{2.13}$$

The beam intensity can also be directly related to the laser power [5] as:

$$I(\vec{r}) = \frac{2P}{\pi\omega(z)^2} e^{\left(\frac{-2r^2}{\omega(z)^2}\right)}, \tag{2.14}$$

where r is the radial distance from the focus, and

$$\omega(z)^2 = {\omega_0}^2 \left[1 + \left(\frac{z}{z_0}\right)^2\right] \tag{2.15}$$

where z the axial distance from the focus, z_0 is the Rayleigh range ($z_0 = \pi{\omega_0}^2/\lambda$), and ω_0 is the beam waist (the radial distance in the focal plane at which the intensity of the beam drops by $1/e^2$). The beam waist was theoretically calculated using a Gaussian beam waist formula ($\omega_0 = \frac{2\lambda}{\pi NA} = 0.222\mu m$).

As mentioned in section 1.2.1, the optical tweezers is only able to trap objects when its pressure-gradient force is greater than its scattering force, or when the ratio R is

$$R = \frac{F_{grad}}{F_{scat}} \geq 1. \tag{2.16}$$

The net trapping force on the trapped object is equal to the gradient force minus the scattering force. The net force in X and Y directions, perpendicular to the trapping beam propagation, should be greater than in the Z direction, along the beam propagation, as the scattering force is much stronger in this direction. However, as stable trapping has been effectively observed through the imaging system and detected through the QPD, the gradient force is assumed to be much greater than the scattering force. Thus, the radial trap stiffness can be simply evaluated using equations 2.12 and 2.14,

$$k_r = -\frac{\partial(\vec{x} \cdot \vec{F}_{grad})}{\partial x} = \frac{32P}{3{\omega_0}^4 c}a^3(n_p - n_m). \tag{2.17}$$

In the data analysis section, this theoretical trapping stiffness is compared with experimental data using multiple laser intensities, according to the table of powers and filter positions in the Data Processing section.

2.2.2 Experimental Calibration Methods

Brownian Harmonic Oscillator

Although the theory is straightforward, the experimental implementation can be difficult, since many problems may arise with the collection of the light [17]. Multiple

preliminary analyses are necessary to evaluate the data from the back focal plane of the condenser and into a quadrant photo-detector. Using a very fine motorized stage, such as a piezoelectric stage, the beam waist can be calculated and the detector sensitivities for each direction of motion can be measured [2][25]. Unfortunately, this study did not calibrate the detector sensitivity and therefore cannot reliably read the QPD data to identify the average displacement of the beads. However, this study is still qualitatively relevant as it relates the laser beam power with the trapping force applied onto the bead.

The Brownian Harmonic Oscillator Method compares the gradient force of the optical tweezers for small displacements relative to the laser focus to a spring. According to Hooke's Law,

$$F_H = -k_{trap}r, \tag{2.18}$$

where k_{trap} is the trapping coefficient relative to the stiffness and efficiency of the trap, shows the linear relation between the displacement of the bead (x) and the force applied on it (F_H). The "Brownian" aspect of this method is the motor of the bead, pushing it in and out of focus in all directions. Small changes in pressure and the movement of the particles surrounding the bead drive the bead in a Brownian (random) motion. However, when trapped, the bead experiences the spring force, and gets overshot towards the laser focus, generating a force against its motion, which creates a harmonic oscillator.

The trapped particles used were $1\mu m$ polystyrene beads, which in the range of the laser beam's wavelength (488 nm) have a refractive index of $\tilde{1}.600$ [8].

Using the Langevin equation [30],

$$M\ddot{x} + \beta\dot{x} + k_r x = \xi(t), \tag{2.19}$$

where M is the mass of the trapping bead, β is the Stoke's drag, k_{trap} is the trapping coefficient, and $\xi(t)$ is the thermal fluctuating force.

The thermal fluctuations term has been formulated [14][25][5] in terms of frequency, and can be described by a Lorentzian profile given by

$$S(f) = \frac{k_B T}{\beta\pi^2(f_c{}^2 + f^2)}, \tag{2.20}$$

where k_B is the Boltzmann constant, T is the temperature, β is the Stoke's drag coefficient defined as

$$\beta = 6\pi\eta a, \tag{2.21}$$

where ν is the viscosity of the medium (distilled water, $\nu = 0.8891$ for room temperature), and a is the bead radius.

f_c is the characteristic frequency, which is directly proportional to the trapping stiffness (k_r), and can be described as

$$f_c = \frac{k_r}{2\pi\beta}. \tag{2.22}$$

The most accurate procedure to analyze the thermal fluctuations of trapped bead is to analyze its Brownian motion recording the data with a position sensing detector, such as a quadrant photodiode, used by this research. Then a power spectrum density (PSD) analysis, which is based on fast Fourier transform models, indicates the magnitude of frequencies present in the fluctuations on the bead.

The characteristic frequency (f_c) plays a key role for the PSD analysis. For frequencies lower than f_c the bead feels the confinement of the tweezers and the PSD is constant. While for higher frequencies, the PSD decays as $1/f^2$ in a characteristic called free diffusion.

Chapter 3

Data Processing

This section addresses the capture and analysis of the data using the Harmonic Oscillator Brownian Motion method.

3.1   Data Visualization

3.1.1   Microscope Eyepiece Imaging

Even though the microscope implemented has an eyepiece and a camera port, it is impossible to view the movement of a trapped object through those. When trapped, the displacements of the bead oscillations are very small. A large displacement from its equilibrium position would cut down the gradient force, allowing the bead to move freely in the sample slide, as opposed to trapped near the focal point of the objective.

The eyepiece is still very useful to locate the available beads in the sample slide in their Brownian motion. Also, the laser light is visible by a reflection from the cover slip. By looking at the beads and the reflection of the laser, it is evident that the beads have a different behavior when close to the incident light. In the eyepiece perspective, the bead moves slowly towards the center of the laser and then becomes motionless, indicating that it is trapped.

Figure 3.1a shows the eyepiece perspective of the visible beads in the eyepiece field of view while one bead is trapped and 3.1b shows the shadow of the trapped bead after the condenser.

3.1.2   What is the Quadrant Photodiode?

In order to track the movement of the trapped particle, a quadrant photodiode (QPD) was purchased. It is composed of four optically active areas separated by a small gap. All of these areas have a semiconductor diode, and when photons of sufficient energy enters the depletion region of the semiconductor, it may strike an atom and release one electron from its atomic structure, as described by the Compton Scattering. This creates a free electron and an "open hole" (an atom with a space for an electron), which will then migrate in opposite directions, due to the electric field across this region. The flow of electrical charges, or current, is proportional to the amount of light entering this semiconductor area. The more light, the more electron-hole pairs, and therefore a bigger photocurrent flows.
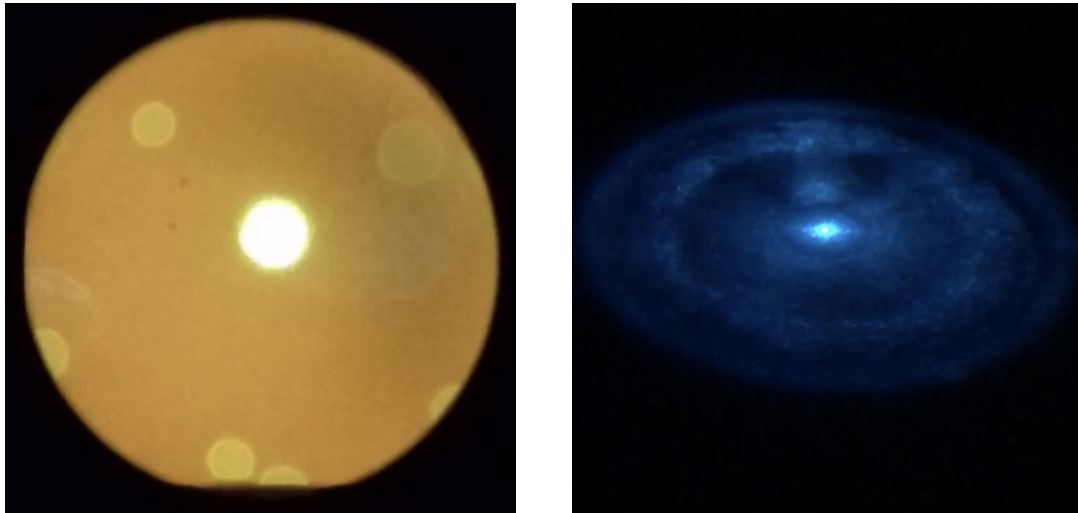
(a) View of the polystyrene beads through the eyepiece. Note that the brightest bead in the middle is trapped and other beads can be seen at the eyepiece field of view.

(b) Shadow of the polystyrene bead when trapped. Note that the bead shadow is located above the brightest point of light and it oscillates around that point.

Figure 3.1: View of the polystyrene beads from the eyepiece and the shadow of the trapped bead after the condenser.

By tracking this photocurrent, photodiodes are able to measure the intensity of the light that hits its detectors. As the QPD is divided in four of these individual semiconductor areas, it is able to track differences in the intensity of light between the four sections. This allows for movement tracking, and calibrating the beam precision. In the optical tweezers setup, after the laser beam hits the trapped bead the light goes through a condenser, which collimates the light onto the QPD detector. Most of the light hitting the trapped bead should be either refracted or absorbed by its material, and therefore, change the intensity of the light hitting the QPD. By tracking the difference in the intensity of the four photocurrents it is possible to evaluate the movement of the trapped bead.
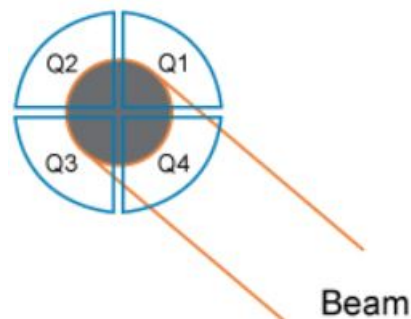
Figure 3.2: Representation of an incident light beam on the 4 identical quadrant-shaped photodiodes

In figure 3.2, it is possible to visualize the positioning of the four photodiodes and their output data can be represented as:

$$Z = SUM = Q1 + Q2 + Q3 + Q4 \tag{3.1}$$

$$X = \frac{(Q2 + Q3) - (Q1 + Q4)}{Q1 + Q2 + Q3 + Q4} = \frac{X_{diff}}{SUM} \tag{3.2}$$

$$Y = \frac{(Q1 + Q2) - (Q3 + Q4)}{Q1 + Q2 + Q3 + Q4} = \frac{Y_{diff}}{SUM} \tag{3.3}$$

If a symmetrical light beam is centered on the QPD, the four photodiodes will induce the same photocurrent, which will result in null difference signals, and the normalized coordinates will have values (X, Y) = (0, 0). If the beam intensity is off-center, different photocurrents will be induced, and thereby difference signals related to the beam displacement will arise. An effort has to be made to understand the shape and intensity profile of the incident beam, as the QPD is sensitive to the power distribution rather than the geometrical center of the beam.

In the optical tweezers setup, the incident beam would have the shadow of the trapped bead in its intensity profile. As found in [28], [25], and [10], the trapping force in the x and y directions should slightly vary, mainly depending on the polarization of the trapping laser beam.

3.1.3   Implementing the Quadrant Photodiode

Implementing the quadrant photodiode into the optical tweezers system was quite challenging as the position sensing detector (PSD) was not purchased, and therefore needed to be developed. Also, the design of the Zeiss microscope did not have an easy access for implementing a detector after the condenser. There was no space to fit a mirror or the QPD itself while the stage was in its lower position, which is necessary to make adjustments on the slide and objective lens and to place new beads. The mirror would only fit underneath the condenser when the slide with new beads, and objective lens were already settled and the stage was in a higher position, close to the position of trapping. The only manner to implement the QPD was by mounting a sliding track with a mirror which reflected the beam onto the QPD. The QPD was mounted in a 3-D stage as in figure 3.3. The sliding track was very demanding, as it required alignment in every run, which is another topic for the Custom-Made setup vs Standard Microscope Setup discussion.

The QPD included a male version of the Hirose 6-pin connector to be powered up and read its output signals. One female version of the Hirose 6-pin was purchased and spliced in order to isolate each pin and connect them to the interface box. The cable jacket had an extra brown cable inside, which was thought to be connected to the case, and therefore be connected to common as pin 5. However, the brown cable was also connected to pin 6, which inputs -5V and when the interface box was turned on, current will go through both cables. This property or malfunction of the female Hirose 6-pin cable jacket motivated the purchase of a new Hirose solder type receptacle [HR10A-7R-6S(73)].

All of the pins were isolated and soldered onto 22-gauge cables, according to the colors in figure 3.4. As in figure 3.5, all of the cables were connected to banana cables at the interface box. 3.5b shows the interface box, which has one column of banana cables connected to the power supply, and another connected to the oscilloscope
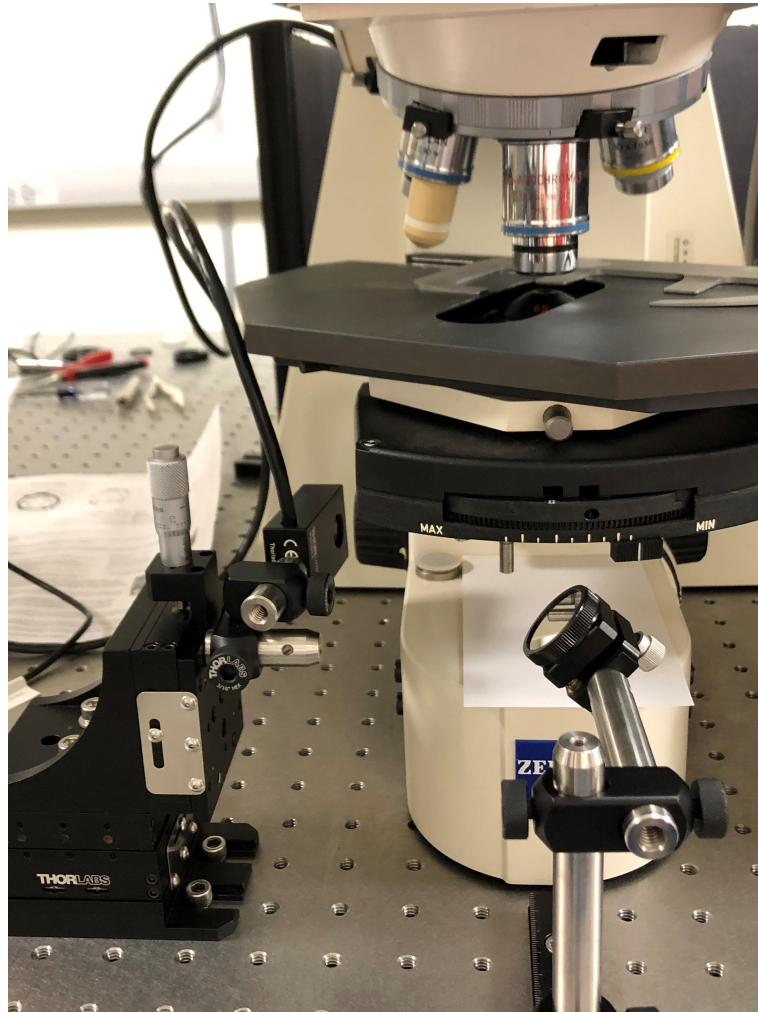
Figure 3.3: QPD Mount at the back focal plane of the condenser. Note that there is a mirror that redirects the light refracted from the bead into the QPD.

Table 3.6 shows the colors of the cables and their input or output signal. Pins 1, 2, and 3 output the signal from the QPD to the oscilloscope, while pins 4, 5, and 6 are connected to the power supply.

3.2   Data Capture

The quadrant photodiode is the detector used to collect the data on the trapped bead's movement and send that information to the oscilloscope through the 6-pin Hirose connector. A MATLAB program, found in Appendix A, was used to read the data from the oscilloscope and plot the voltage outputted from the QPD vs time. A round continuously-variable filter was used to modify the beam intensity of the laser and visualize the behaviors of the trapped bead. As discussed in the Harmonic Oscillator Brownian Motion section, the power of the laser and the frequency of the bead through the focus should be linear.

The laser used as the incident light in the system is a Coherent blue (488 nm) laser, which outputs 100 mW in power. As shown in table 2.2, beamsplitter #5 is the one that transmits the most light and was the one used by this study. Table
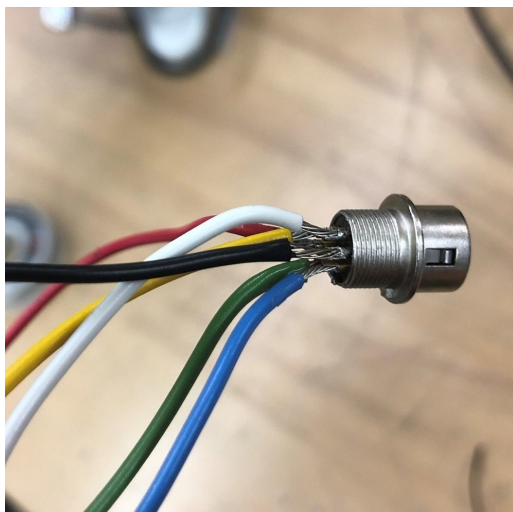
(a) Hirose 6-pin connector to the Quadrant Photodiode. Note that all of the wires are color coded according to figure 3.4b
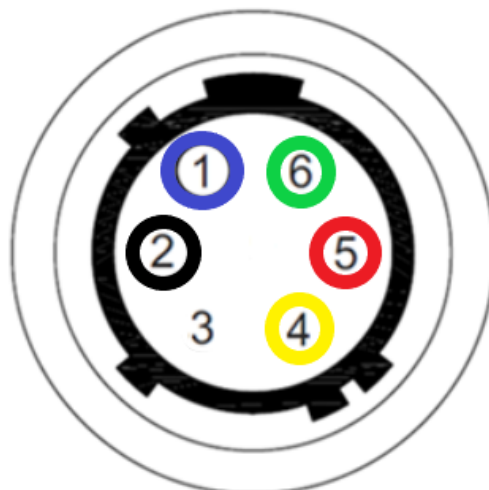
(b) Representation of the colors of cables used to connect the QPD to the interface box

Figure 3.4: Representation of the cables colors used on the QPD connector to the interface box
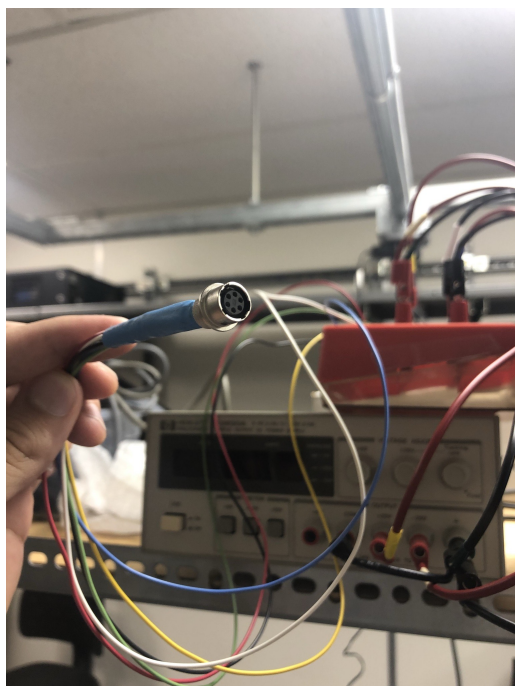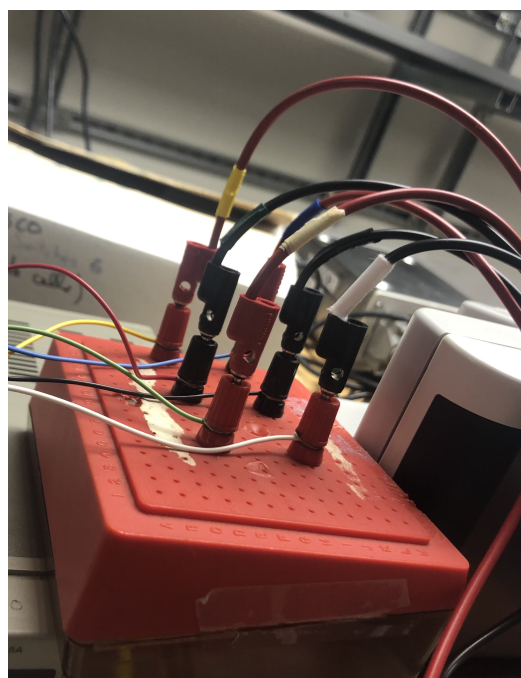
(a)   (b)

Figure 3.5: Figures of QPD's Hirose 6-pin connector cable and its interface box. Note that the banana cables were plugged into a power supply and an oscilloscope.

3.7 shows the relationship between the filter position and the laser power after the objective lens, active incident light power onto the trapped object.

Multiple data sets were analyzed with different filter settings. Each data set consists of X, Y, and Z data points, which are described in 3.6. As discussed in

Pin	Color	Input/Output Signal
1	Blue	X-Axis $[Q2 + Q3] - [Q1 + Q4]$
2	Black	Y-Axis $[Q1 + Q2] - [Q3 + Q4]$
3	White	SUM $[Q1 + Q2 + Q3 + Q4]$
4	Yellow	+5V
5	Red	Common
6	Green	-5V

Table 3.6: Input and output signals from all isolated pins on the QPD

Filter Position	Power (mW)
0	40.3
90	24.3
100	15.8
110	9.22
120	5.61
130	3.29
140	2.05
150	1.28
160	0.84
170	0.55

Table 3.7: Laser Power after the objective lens using multiple filter positions. Note that as the position of the filter increases more light gets blocked and the laser power through the objective lens decreases.

the methods section, each direction may have a distinct trapping stiffness. The trapping stiffness in the axis perpendicular to the laser (X, and Y) may vary due to the polarization of the laser, while the axial direction Z has its stiffness decreased by the photons that are scattered and reflected from the bead.

3.3   Data Analysis

The MATLAB code, which can be found in Appendix A, was written to communicate with the oscilloscope and read the QPD output and plot the output versus time. Another piece of code, which can be found in Appendix B, is responsible for processing these data sets, and quantitatively analyze them by outputting a standard frequency. The data processing code reads the data sets, averages data points to decrease noise, creates a fast Fourier transform (FFT) of the data set, and makes a weighted average to find the standard frequency.

In order to evaluate if the QPD output was an accurate representation of the movement of the bead, the first data set analyzed did not contain a trapped bead. This data set was compared with trapped bead data, in which the power was manipulated to analyze the behavior of the bead. Clearly, as shown in figure **??**, the voltage output from the QPD is truly different when there is a trapped bead and when there is not. This identifies that the voltage output from the QPD reflects the movement of the trapped bead, and when there is no bead, the voltage output is

fairly constant.
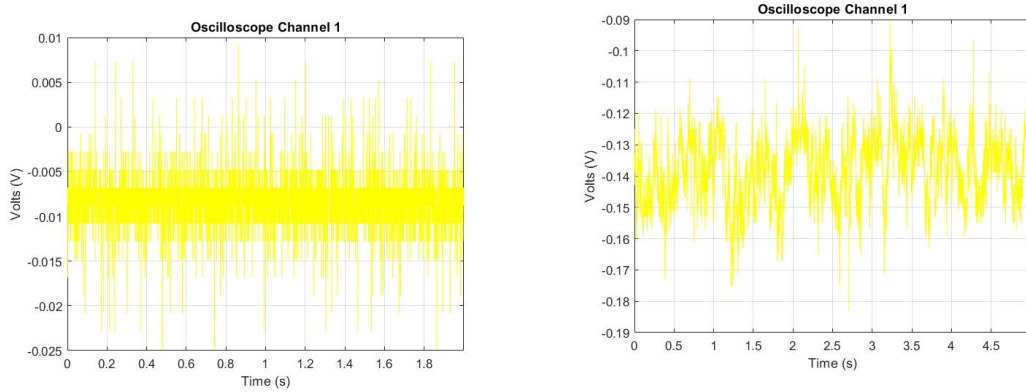
(a) QPD voltage output plot of no trapped bead data set.

(b) QPD x-axis voltage output plot of a trapped bead with the filter at position 110.

Figure 3.8: QPD Output plot of Voltage vs Time with and without a trapped bead. Note that the image on the left, which represent a "no trapped bead" data set, shows a constant voltage around -0.01, while the image on the right, which shows a trapped bead data set, oscillates its voltage output as the bead moves in the focal region.

Subsequently, the power of the incident beam was modified to observe the behavior of the bead. As discussed in the methods section, more laser power should increase the forces applied in the trapped bead. Both of the thermal fluctuating terms (ξ), and the harmonic oscillator term (k_r) in the Langevin equation should increase as the laser power is stronger. The only unaffected term in that equation is the Stoke's drag term (β), which is not dependent on the laser power. However, the Stoke's drag term only acts as a frictional force and does not drive or generate motion, but acts as a resistance to the bead's motion.

As seen in equation 2.22, the characteristic frequency (f_c) is directly proportional to the trapping stiffness coefficient (k_r). Even though the standard frequency processed is not equivalent to the characteristic frequency, it can still be compared and used to understand the behavior of the beads in this Optical Tweezers system. The standard frequency aims to agree with the characteristic frequency, but there are multiple factors that need to be analyzed in order to view their discrepancies.

According to [9], by generating a power spectrum density (PSD) analysis in equation 2.20 should identify the characteristic frequency (f_c) for low frequencies, as the PSD should be constant, and then decay as $1/f^2$ for higher frequencies. However, in order to accurately generate a PSD in a quadrant photodiode data set, the QPD should collect all of the laser light refracted by the sample, which in this experiment was not possible, due to the structure of the commercial microscope used (this issue is analyzed in the discussion section). Also, the data sets were taken with a frame rate of 1000 Hz, which would limit the PSD analysis to the 500 Hz range, however the PSD analysis found in multiple sources [9] [25] [14] collected the power of 2 or 3 orders of magnitude higher than the 1000Hz frame rate, which would require a much higher detector bandwidth.

However, even though the QPD calibration was not completed and the QPD only partially collected the light refracted from the sample, valuable data could be

analyzed. An increase in the laser power resulted in an increase of the standard frequency outputted from the data sets recorded. Figure 3.9 shows the correlation between the laser power and the standard frequency outputted from the data processing MATLAB code.
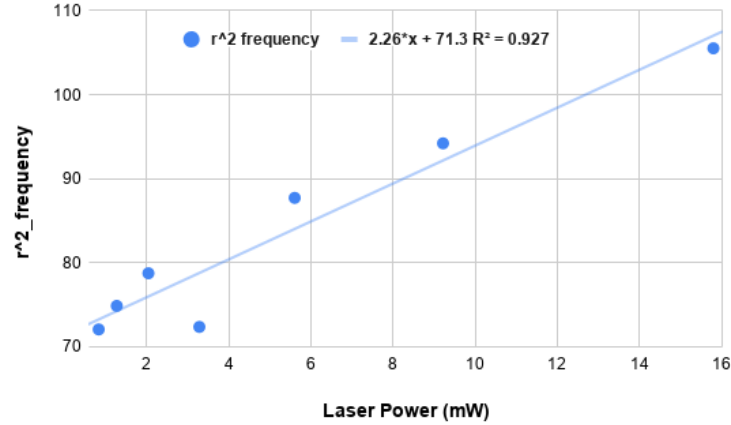
Figure 3.9: Radial frequency by Laser Power. Note that there is a linear correlation ($R^2 = 0.927$) between the frequency of the bead and the laser power.

The standard frequencies generated by the FFT were used to generate radial trapping stiffness coefficients (k_r), according to equation 2.22. These coefficients were collected and compared with the theoretical trapping coefficient, according to equation 2.17. Figure 3.10 demonstrates the data sets collected using the Brownian Harmonic Motion and the Rayleigh regime methods. Although the experimental data sets collected do not reflect the theoretical rate of change, both data sets are in the same order of magnitude and correspond to a linear increase.
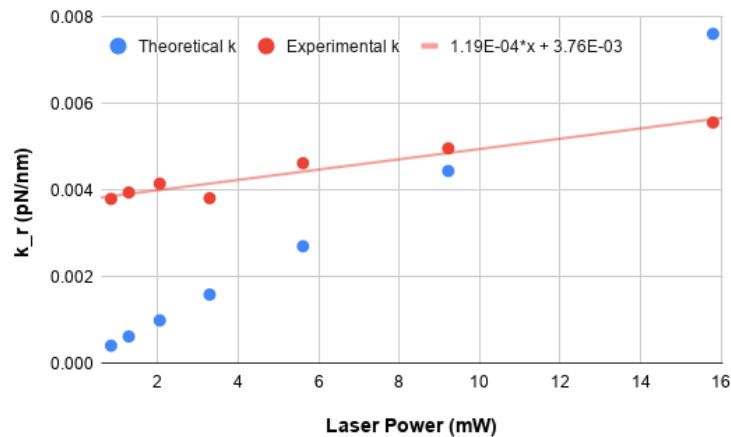
Figure 3.10: Experimental and Theoretical trapping stiffness vs Laser Power.

As discussed in the theoretical methods of calibration section, the Rayleigh regime does cover trapping objects in the size of the polystyrene beads used ($d = 1\mu m$). However, the theoretical methods of calibration for beads that are within the range of the wavelength of the laser beam ($a \approx \lambda$) require rigorous approaches, such as the Generalized Lorentz-Mie scattering or the T-Matrix theory. These

approaches, as well as the geometrical optics regime approach, are beyond the scope of this thesis. Nonetheless, the two methods used by this thesis to numerically represent the trapping stiffness of the Optical Tweezers project at Drew University agree within an order of magnitude of accuracy for all data points.

Chapter 4

Discussion

4.1 Custom vs Commercial Microscope

This section will compare the 2019 OT system and the current OT system, by pointing out their similarities and differences and the advantages of each system. Although the new Zeiss microscope has brought many benefits to the current system, there are multiple drawbacks that need to be analyzed between this setup and the custom-made setup used in 2019.

Most of the optical equipment used in the 2019 OT system, including laser, mirrors, lenses, and filters were maintained and adapted to the new setup. However, the main part of the system, where trapping occurs, was switched from a custom-made setup with a 3D-stage for the sample. The laser beam was redirected onto the stage by a dichroic mirror and the sample was viewed by a cell-phone camera imaging system, which were supported by two vertically mounted metric rails. The current system replaced the stage, dichroic mirror, and imaging system to a Zeiss Axioplan 2 microscope that has all of those tools integrated in one bulky piece of equipment.

The biggest advantage of using the commercial microscope is related to the ease in alignment, the incident light port, the dichroic mirrors, and the objective lens are aligned by the default configuration of the microscope. Also, the condenser underneath the stage can be quite easily aligned and its position can be tweaked for slight movements on the focal point of the incident beam for the best data visualization. The microscope provides a camera port and adapter as well, therefore a video analysis system can be integrated easily.

The advantages of having a custom-made system, would be its modular abilities. As the microscope is a bulky piece of equipment it could be quite difficult to integrate a new functionality or part into the "trapping zone". For example, the QPD system was very difficult to be integrated below the stage, underneath the condenser. Even though multiple filters and lenses used to manipulate the white light source that illuminates the sample were removed, the space for a mirror to be implemented to reflect the tweezers data to the QPD was very restricted. As multiple parts were also removed, irremovable adjustment structures limited even more the space for a new mirror, they partially or fully blocked the image reflected onto the mirror before reaching the QPD.

In a custom system such as the one in 2019, more parts and functionalities are easier to be incorporated as the parts can be moved or even replaced. New rails, adaptors, and spacers can be maneuvered to create or remove space between parts

and even introduce new functionalities to the system. For example, in a custom setup a new laser could be added, creating a double-laser OT system by adding the necessary parts. Although each part would have to be carefully placed and individually aligned, a custom-made setup would still make these changes possible.

While transitioning to a setup with a fixed commercial microscope system, the addition of new functionalities, not supported by the microscope, could be either very difficult or impossible. For instance, to have a better detection of the QPD Output Voltage data sets, the condenser must collimate the light from the sample for the light to be easier to be redirected to the QPD. The only way of increasing the collimation would be by replacing the condenser lens to a higher NA lens. However, the mount for the condenser lens is not a conventional mount, which did not allow for the replacement of the condenser lens with one existing lens in the department. Similarly, the replacement of the objective lenses, dichroic mirrors, and filters contained in the microscope would only be possible if the exact parts for that specific microscope would have been purchased.

4.2 Future Optical Tweezers Applications at Drew University

In this section, multiple projects that are applicable in the optical tweezers in the short and long terms will be discussed and analyzed.

4.2.1 Calibration of the Quadrant Photodiode

As previously explained, a quadrant photodiode outputs a voltage signal directly proportional to the light power received at the detectors area. This voltage output should also be linearly proportional to the position of the trapped bead. In other words, a movement of the trapped bead should reflect in a proportional change of the voltage output signal in the direction of the bead's movement. An explanation of how the QPD outputs its voltage signals can be found in the data processing section, and the definition of these signals are found in table 3.6.

In order to numerically analyze the displacement of the trapped beads, there are proportionality coefficients in both x and y directions, which relate the output voltage with the displacement of the trapped bead. There are simple linear relations (in particle displacement intervals of $\tilde{2}00$ nm around the trap center [5]), as $V = C_x x$ and $V = C_y y$, where C_x and C_y are the coefficients that relate voltage to displacement (in V/nm).

To determine these coefficients, beads of known size and material are firmly attached to the sample slide, and they are moved using a very fine motorized stage, such as a piezoelectric stage. The bead displacement should also cause a deflection on the direction of the refracted light, altering the QPD output voltage. By moving the bead by known displacements, and observing the voltage outputted it is possible to calculate the proportionality coefficients (C_x and C_y). This calibration is crucial for precise calibration of the trapping stiffness, as the displacement of the trapped object can only be calculated through this process. It plays a central role in the linear viscous drag, and the equipartition theorem calibration methods, also discussed in this paper.

4.2.2   Parameters Variations

In order to analyze the reliability of the optical trapping, the parameters of trapping should be changed and compared. Changing the size of the beads, ranging from Rayleigh particle's size to Mie Theory particle's size, the refractive index of the beads (different materials), and the viscosity of the media.

Changing the size of the beads to the Rayleigh range would be very interesting, as it would allow to analyze the appearance of the image of the beads through the eyepiece and camera port. Also, it would be very interesting the view the variations in the data capturing by the Quadrant Photodiode and how a smaller bead would alter the output voltage provided by the QPD. It would also contribute to the use of new theoretical calibration methods. Rayleigh range sized particles have multiple theoretical methods and analyses on their calibration and optical tweezers force.

Another interesting variation in the parameters currently in place would be modifying the wavelength of the laser beam. By changing the current laser (488nm) to a higher wavelength near the infrared range would decrease the absorption of light in the water (medium), and on the trapped particle. Using a near infrared range, would permit the trapping of biological samples as the light would not be absorbed by the sample and therefore not be damaged by the laser beam.

4.2.3   Geometrical Optics Regime

Unlike the previous section this method is only appropriate for large beads, that is:

$$2ka(m-1) \gg 1, \tag{4.1}$$

which for typical situations, can be simplified to $a \gg \lambda$. In these parameters, the geometrical optics regime is valid and can be used to calculate the force exerted by an optical tweezers on the bead.

To accurately derive the trapping stiffness using geometrical ray optics, the reflection and transmission of a single ray interacting with the trapped object is studied. This single ray can either be reflected by the first surface of the object, or be transmitted into the object and reflected internally numerous times (or none) until it leaves the trapped object in a new direction. The probability of these infinite number of cases is calculated, which is dependent on the shape and index of refraction of its material and the medium, to accurately represent the result of a single ray optical tweezers. Then, this result becomes an integrand, and is integrated to accurately represent the entire beam. This result takes into account the Gaussian shape of the laser beam, and the spherical aberrations due to the optical components.

Even though many sources [11][19][16] have quantitatively described and analyzed this method, this analysis is mathematically complex and beyond the scope of this paper. The sources mentioned, although not analytically used by this study, could be of great assistance in the future, if the chosen trapping objects have a much greater size than the incident laser beam wavelength.

4.2.4   Linear Viscous Drag Method

The Viscous Drag method is an experimental calibration method based on Stoke's Law:

$$F_d = 6\pi\eta a\nu, \tag{4.2}$$

where F_d is the frictional force, known as Stoke's drag, η is the medium dynamic viscosity, a is the radius of the trapped bead, and ν is the flow velocity relative to the surrounding solution. When the stage is moved, a trapped bead will experience Stoke's drag, and be displaced from the focal region, its equilibrium position. The optical tweezers trapping force can be compared with a harmonic oscillator system for small displacements, therefore there is a counteractive linear force acting on the bead. According to the equation 2.18, the trapping force will counteract the Stoke's drag force and, with ideal conditions, keep the bead stable at some displacement r to the focal region.

There is a linear relation between the speed of the stage and the displacement of the trapped bead relative to the focal region. The faster the stage is moving, higher are the Stoke's drag and the Hooke's law resistance force. By isolating the spring coefficient, the trapping efficiency (in N/m) can be written as:

$$F_d = F_H \rightarrow k_{trap} = -\frac{6\pi\eta a\nu}{r}. \tag{4.3}$$

The displacement of the bead from the focal region (r) can be found either by a calibrated QPD, or by the mean of the squared displacement through the equipartition theorem, found in the following section.

Without a QPD, or an imaging system that precisely tracks the position of the trapped bead, it is still possible to determine the trapping force of a setup using this method. Using a fine motor and increasing the speed of stage until the flow velocity relative to the solution (ν) is fast enough that the drag force would push the bead away for the laser focus, ceasing the trapping. At this point, it is possible to find an upper bound in the trapping force using equations 2.18 and 4.2 as:

$$F_H \leq F_d \rightarrow F_H \leq 6\pi\eta a\nu_{max}, \tag{4.4}$$

where ν_{max} is the maximum flow velocity relative to the solution (the speed of the stage). By changing the power of the incident laser beam, there should be a linear relation between the laser power and maximum flow velocity relative to the media (ν_{max}), and consequently with the drag force (F_d) as well.

Unfortunately, the stage available in the Zeiss Microscope, currently in this setup, is not motorized and very imprecise and rough. As it is not motorized, it is not able to be moved in constant and known speeds. Using a graded (dashed) microscope slide and an imaging software, it is possible to determine the velocity of the slide using variable speeds and moving the stage manually. However, the stage available for the setup is very imprecise, and moving the stage to one direction can affect the movement of other directions and even drive the trapped bead out of the trapping region.

4.2.5   The Equipartition Theorem Method

The equipartition theorem method is one of the simplest methods of calibrating an optical tweezers, however it is the least accurate of all methods discussed in this paper. It also can be used to assist other calibrating methods, by determining some variables such as the average displacement of the bead, the average velocity of the medium. The equipartition theorem relates the temperature of a system to each degree of freedom that is quadratic in energy. It equates each degree of freedom

with $\frac{1}{2}k_B T$, where k_B is the Boltzmann constant and T is the absolute temperature. In optical tweezers, the displacement of the trapped bead can be compared to a spring, with potential energy $V = \frac{1}{2}k_{trap}r^2$, a quadratic harmonic oscillator.

As the radial displacement constant r contains two degrees of freedom (X and Y), it contributes as two $\frac{1}{2}k_B T$ terms. This calibration method can be written as:

$$U_H = U_T \rightarrow k_{trap} = \frac{2k_B T}{\langle r^2 \rangle}, \tag{4.5}$$

where $\langle r^2 \rangle$ is the mean of the squared displacement from the trapping center.

The temperature effects caused by the irradiation of the focused laser beam in the power range (100mW) used by this research are less than a few kelvins [3]. Therefore, the use of the room temperature (298K) is valid for this system.

Unfortunately, this current setup is not able to quantify the displacement of a trapped bead. In order to find the displacement of a trapped bead using a QPD, the position sensitivity of the detector needs to be calibrated. , but this is a new method that can be explored in the future.

Chapter 5

Conclusion

Optical Tweezers is a scientific instrument created by Dr. Arthur Ashkin in the early 1970's at the New Jersey branch of Bell Labs. It is simply composed by a high power laser, with Gaussian shaped beam, and a high numerical aperture objective lens. By placing micro or nano sized particles around the focal region of the objective lens, it is possible to trap and manipulate these particles using light. Optical Tweezers systems have several applications in biology, as biological samples, such as: viruses, bacteria, proteins, and strands of DNA can be analyzed in the trap. Also, as it can describe with high accuracy the behavior of nano sized particles, it has many applications on nanotechnologies, and on quantum physics research.

There are several forces applied to a particle when trapped in a optical tweezers. Additionally, there are multiple approaches to describe these forces on a particle, depending on its size, such as the Rayleigh regime, and the geometric optics regime discussed in this study. As light imparts momentum, a change in the light momentum reflects in a change in the momentum of the medium or of the surface that the light strikes. In systems where the trapped particles are spherical, and the index of refraction of the particle (n_b) is greater than the media's (n_m), $m > 1$, the net momentum of the light points outwards due to the Gaussian shape of the laser beam. Therefore, there is a net momentum, and a force, on the particle, which always points towards the focal region of the objective lens, trapping the particle.

At Drew University, optical tweezers systems were first studied at Dr. Larson's optics lab in the 2019 Drew Summer Science Institute. Due to a unexpected pause in the line-scanning confocal microscopy project, the research group decided to build an optical tweezers, as most of the components necessary were available in the Drew Physics department. By the end of the summer research period, videos were recorded establishing trapping and manipulation of 1 μm polystyrene beads. However, there was not enough time in the research period to calibrate the optical tweezers, and determine the trapping stiffness of the system.

In the Fall of 2020, optical tweezers research at Drew University were resumed with the goal of the calibration of its trapping stiffness. A Zeiss microscope, which was donated to the Drew Physics department in the meantime, was decided to be implemented in the optical tweezers setup. The microscope is a bulky piece of equipment, and brought some advantages and drawbacks to the system comparing with the 2019 DSSI setup.

This paper describes multiple calibration methods and analyzes two of them, the Rayleigh regime, and Brownian Harmonic Oscillator methods, to quantitatively

describe the trapping stiffness of the system. The Rayleigh regime is not suitable for the particle size used by this research, but it gives a valuable trapping stiffness approximation, as used in many other sources. Also, the theoretical calibration methods that precisely determine the trap stiffness for the particle size used in this research are far beyond the scope of this paper. Therefore, due to the complexity of theoretical calibration methods, experimental calibration of optical tweezers is often preferred.

The data calculated using the Rayleigh Regime is compared with the experimental data using the Brownian Harmonic Oscillator method. The Brownian Harmonic Oscillator requires a position sensing detector, which in this case is a quadrant photodiode (QPD), to analyze the motion of a trapped bead. The data outputted from the QPD was then evaluated by a Fast Fourier Transform MATLAB code, which outputted a standard frequency, according to the power of the laser. As expected the frequency of the bead motion was higher as the laser power increased. Then, the standard frequency was assumed to be the characteristic frequency (f_c) for that laser power, and a trapping stiffness coefficient was then calculated. Both of the coefficients from the Rayleigh Regime and Brownian Harmonic Oscillator, although not sharing the same linear rate, were in the same order of magnitude ($10^{-3} pN/nm$).

Although the data from both theoretical and experimental approaches correlate, there are several areas in their analysis that can be improved, and the trapping stiffness more precisely determined. Measuring the beam waist experimentally, other than theoretically could improve the Rayleigh Regime data. The Brownian Harmonic Oscillator data can be more precisely determined by a faster sample rate detection, which would allow for a better power spectrum density analysis. Furthermore, the QPD should be calibrated and should be exposed to the entirety of the refracted laser beam after the condenser, while it is currently only partially exposed.

Also, there are several applications that can be implemented to this optical tweezers system in the near future. Multiple calibration methods can be analyzed and their data compared with the current methods, by using a piezoelectric stage to calibrate the QPD, and measure the beam waist of the trap. Parameters variations, such as different laser wavelength, bead sizes, bead and medium refractive indices, and medium viscosity could increase the reliability of the calibrated trapping stiffness and allow for the study of many optical tweezers' behaviors.

Appendix A

Appendix A

A.1   QPD Data Capture MATLAB Code

```matlab
%% Example to connect to and download waveform
% data from an oscilloscope
% This example connects to an Agilent
% scope using VISA and sends SCPI
% commands to initiate acquisition and downloads the data
% and displays it in MATLAB
%
% Note that this demo requires Agilent IO Libraries installed.
% The VISA resource string to the oscilloscope
% is to be obtained from Agilent connection expert.
%
% Copyright 2010 The MathWorks, Inc
%% Interface configuration and instrument connection

% connect to scope
% The second argument to the VISA function
% is the resource string for your instrument
scope=instrfind('Type', 'visa-usb', 'RsrcName',
    'USB0::0x0957::0x1798::MY54100989::0::INSTR', 'Tag', '');

if isempty(scope)
    scope = visa('agilent',
    'USB0::0x0957::0x1798::MY54100989::0::INSTR');
else
    fclose(scope)
    scope=scope(1);
end
% Set the buffer size
scope.InputBufferSize = 100000;
% Set the timeout value
scope.Timeout = 10;
% Set the Byte order
scope.ByteOrder = 'littleEndian';
```

```matlab
% Open the connection
fopen(scope);
%% Instrument control and data retrieval

% Data collection for Channel 1

    % Reset the instrument and autoscale and stop
    fprintf(scope,'linspace(-500e-06,500e-06,100)');
    fprintf(scope,':STOP');
    % Set timebase to main
    fprintf(scope,':TIMEBASE:MODE MAIN');
    % Set up acquisition type and count.
    fprintf(scope,':ACQUIRE:TYPE NORMAL');
    fprintf(scope,':ACQUIRE:COUNT 1');
    % Specify number of data points desired by :WAV:DATA?
    fprintf(scope,':WAV:POINTS:MODE RAW');
    fprintf(scope,':WAV:POINTS 5000');
    % Now tell the instrument to digitize channels
    fprintf(scope,':DIGITIZE ');
    % Wait till complete
    operationComplete = str2double(query(scope,'*OPC?'));
    while ~operationComplete
        operationComplete = str2double(query(scope,'*OPC?'));
    end
    % Get the data back as a WORD (i.e., INT16),
    % other options are ASCII and BYTE
    fprintf(scope,':WAVEFORM:FORMAT WORD');
    % Set the byte order on the instrument as well
    fprintf(scope,':WAVEFORM:BYTEORDER LSBFirst');
    % Get the preamble block
    preambleBlock = query(scope,':WAVEFORM:PREAMBLE?');
    % The preamble block contains all of the
    % current WAVEFORM settings.
    % It is returned in the form <preamble_block><NL>
    % where <preamble_block> is:
    % FORMAT : int16 - 0 = BYTE, 1 = WORD, 2 = ASCII.
    % TYPE : int16 - 0 = NORMAL, 1 = PEAK DETECT, 2 = AVERAGE
    % POINTS : int32 - number of data points transferred.
    % COUNT : int32 - 1 and is always 1.
    % XINCREMENT : float64 - time difference between data points.
    % XORIGIN : float64 - always the first data point in memory.
    % XREFERENCE : int32 - specifies the data point
    %                       associated with x-origin.
    % YINCREMENT : float32 - voltage diff between data points.
    % YORIGIN : float32 - value is the voltage at center screen.
    % YREFERENCE : int32 - specifies the data point
    %                       where y-origin occurs.
    % Now send commmand to read data
```

```matlab
% Specify data from Channel
fprintf(scope,':WAVEFORM:SOURCE CHAN1');
fprintf(scope,':WAV:DATA?');
% read back the BINBLOCK with the data in
% specified format and store it in
% the waveform structure. FREAD removes
% the extra terminator in the buffer
waveform.RawData1 = binblockread(scope,'uint16');
fread(scope,1);
% Read back the error queue on the instrument
instrumentError = query(scope,':SYSTEM:ERR?');
while ~isequal(instrumentError,['+0,"No error"' newline])
    disp(['Instrument Error: ' instrumentError]);
    instrumentError = query(scope,':SYSTEM:ERR?');
end

%Close the VISA connection.
fclose(scope);

%% Data processing the data retrieved from the scope
% Extract the X, Y data and plot it

% Maximum value storable in a INT16
maxVal = 2^16;

%  split the preambleBlock into individual pieces of info
preambleBlock = regexp(preambleBlock,',','split');

% store all this information into a waveform
% structure for later use
waveform.Format = str2double(preambleBlock{1});
% This should be 1, since we're specifying INT16 output
waveform.Type = str2double(preambleBlock{2});
waveform.Points = str2double(preambleBlock{3});
waveform.Count = str2double(preambleBlock{4});
% This is always 1
waveform.XIncrement = str2double(preambleBlock{  5});
% in seconds
waveform.XOrigin = str2double(preambleBlock{6});
% in seconds
waveform.XReference = str2double(preambleBlock{7});
waveform.YIncrement = str2double(preambleBlock{8});
% V
waveform.YOrigin = str2double(preambleBlock{9});
waveform.YReference = str2double(preambleBlock{10});
waveform.VoltsPerDiv = (maxVal * waveform.YIncrement / 8);
% V
waveform.Offset = ((maxVal/2 - waveform.YReference)
```

```matlab
* waveform.YIncrement + waveform.YOrigin);   % V
waveform.SecPerDiv = waveform.Points *
waveform.XIncrement/10 ; % seconds
waveform.Delay = ((waveform.Points/2 -
waveform.XReference) * waveform.XIncrement
+ waveform.XOrigin); % seconds

% Generate X & Y Data
waveform.XData1 = (waveform.XIncrement.*
(1:length(waveform.RawData1))) - waveform.XIncrement;
waveform.YData1 = (waveform.YIncrement.*
(waveform.RawData1 - waveform.YReference))
+ waveform.YOrigin;

% Plot it
figure(1);
plot(waveform.XData1,waveform.YData1, 'y');
set(gca,'XTick',(min(waveform.XData1):
waveform.SecPerDiv:max(waveform.XData1)))
xlabel('Time (s)');
ylabel('Volts (V)');
title('Oscilloscope Channel 1');
grid on;

%% Reopen for New Channel
fopen(scope);

fprintf(scope,':WAVEFORM:SOURCE CHAN2');
fprintf(scope,':WAV:DATA?');
% read back the BINBLOCK with the data
% in specified format and store it in
% the waveform structure. FREAD removes
% the extra terminator in the buffer
waveform.RawData2 = binblockread(scope,'uint16');
fread(scope,1);
% Read back the error queue on the instrument
instrumentError = query(scope,':SYSTEM:ERR?');
while ~isequal(instrumentError,['+0,"No error"' newline])
    disp(['Instrument Error: ' instrumentError]);
    instrumentError = query(scope,':SYSTEM:ERR?');
end

%Close the VISA connection.
fclose(scope);

 % Generate X & Y Data
waveform.XData2 = (waveform.XIncrement.*
(1:length(waveform.RawData2))) - waveform.XIncrement;
```

```matlab
waveform.YData2 = (waveform.YIncrement.*
(waveform.RawData2 - waveform.YReference))
+ waveform.YOrigin;

% Plot it
figure(2);
plot(waveform.XData1,waveform.YData2, 'g');
set(gca,'XTick',(min(waveform.XData2):
waveform.SecPerDiv:max(waveform.XData2)))
xlabel('Time (s)');
ylabel('Volts (V)');
title('Oscilloscope Channel 2');
grid on;

%% Reopen for New Channel
fopen(scope);

fprintf(scope,':WAVEFORM:SOURCE CHAN3');
fprintf(scope,':WAV:DATA?');
% read back the BINBLOCK with the
% data in specified format and store it in
% the waveform structure. FREAD removes
% the extra terminator in the buffer
waveform.RawData3 = binblockread(scope,'uint16');
fread(scope,1);
% Read back the error queue on the instrument
instrumentError = query(scope,':SYSTEM:ERR?');
while ~isequal(instrumentError,['+0,"No error"' newline])
    disp(['Instrument Error: ' instrumentError]);
    instrumentError = query(scope,':SYSTEM:ERR?');
end

%Close the VISA connection.
fclose(scope);

 % Generate X & Y Data
waveform.XData3 = (waveform.XIncrement.*
(1:length(waveform.RawData3))) - waveform.XIncrement;
waveform.YData3 = (waveform.YIncrement.*
(waveform.RawData3 - waveform.YReference))
+ waveform.YOrigin;

% Plot it
figure(3);
plot(waveform.XData1,waveform.YData3);
set(gca,'XTick',(min(waveform.XData3):
waveform.SecPerDiv:max(waveform.XData3)))
xlabel('Time (s)');
```

```matlab
    ylabel('Volts (V)');
    title('Oscilloscope Channel 3');
    grid on;

    % Delete objects and clear them.
    delete(scope); clear scope;
```

A.2   QPD Data Processing MATLAB Code

```matlab
%% Optical Tweezers Data Processing

%Open the matlab figure with figure's name
fig = openfig('Tweezers_5Data2_Xaxis_F100.fig', 'visible');
% Data set from the Calibration Code

% Access the plotted graphics objects through
% the Children properties.
% The Axes objects are children of the figure.
% The plotted graphics objects are typically
% children of the Axes object.
axObjs = fig.Children;
dataObjs = axObjs.Children;

% The 'dataObjs' array that appears in the
% Command Window indicates the types of
% graphics objects in the axes.
% Different graphics objects store data differently.
% If the first element in 'dataObjs' is a
% Line object, then access its data using this code.
x = dataObjs(1).XData;
y = dataObjs(1).YData;
z = dataObjs(1).ZData;

%% Smooth out intensity values with rolling average

for index = 1:4999
    if index <= 11
        sum = 0;
        for q = 0:10
            sum = sum + y(index + q);
        end
        areaAverage = sum/10;
        if areaAverage - 0.1 > y(index)
            if index == 1
                y(index) = (y(index + 1) + y(index + 2))/2;
            else
                y(index) = (y(index - 1) + y(index + 1))/2;
            end
```

```matlab
        end
    elseif 11 < index && index <= 4999
        sum = 0;
        for q = 1:10
            sum = sum + y(index - q);
        end
        areaAverage = sum/10;
        if areaAverage - 0.1 > y(index)
            y(index) = (y(index - 1) + y(index + 1))/2;
        end
    end
end

plot(x, y)

%% Create Fast Fourier Transform Data ONE SIDED
n = length(x);
FT = fft(y)/n;
FT(1) = 0;
% Number of data points in a second (Sample frequency)
Ts = x(2) - x(1);
fs = 1/Ts;
fn = fs/2;
f = (0:length(FT)-1)*fs/length(FT);

% Plotting
fv = linspace(0,1, fix(n/2)+1)*fn;
Iv = 1:length(fv);
plot(fv,abs(FT(Iv))*2)
xlabel('Frequency (Hz)')
ylabel('Magnitude')

% Average frequencies with the big magnitudes,
k = 1;
sum = 0;
while k <= length(FT(Iv))
    sum = sum + abs(FT(k)) * fv(k);
    k = k + 1;
end
avg = round(sum*n/k);
fv(avg) % Outputs the characteristic frequency for each data set
```

Bibliography

[1]   A. Ashkin et al. "Observation of a single-beam gradient force optical trap for dielectric particles". In: *Opt. Lett.* 11.5 (May 1986), pp. 288–290. DOI: 10.1364/OL.11.000288. URL: http://ol.osa.org/abstract.cfm?URI=ol-11-5-288.

[2]   Arnd Pralle et al. "Thre...dimensional higˆresolution particle tracking for optical tweezers by forward scattered light". In: *Microscopy Research and Technique* 44 (1999).

[3]   Peter M. Celliers and Jérôme Conia. "Measurement of localized heating in the focus of an optical trap". In: *Appl. Opt.* 39.19 (July 2000), pp. 3396–3407. DOI: 10.1364/AO.39.003396. URL: http://ao.osa.org/abstract.cfm?URI=ao-39-19-3396.

[4]   P. A. Maia Neto and H. M Nussenzveig. "Theory of optical tweezers". In: *Europhysics Letters (EPL)* 50.5 (June 2000), pp. 702–708. ISSN: 1286-4854. DOI: 10.1209/epl/i2000-00327-4. URL: http://dx.doi.org/10.1209/epl/i2000-00327-4.

[5]   Paul Bartlett and Stuart Henderson. "Three-dimensional force calibration of a single-beam optical gradient trap". In: *Journal of Physics: Condensed Matter* 14.33 (Aug. 2002), pp. 7757–7768. DOI: 10.1088/0953-8984/14/33/314. URL: https://doi.org/10.1088/0953-8984/14/33/314.

[6]   A. Mazolli, Paulo Maia Neto, and Herch Nussenzveig. "Theory of trapping forces in optical tweezers". In: *Royal Society of London Proceedings Series A* 459 (Dec. 2003), pp. 3021–3041. DOI: 10.1098/rspa.2003.1164.

[7]   Steven Chu. *Conversations with History: An Interview with Steven Chu.* 2004. URL: http://globetrotter.berkeley.edu/people4/Chu/chu-con4.html.

[8]   Xiaoyan Ma et al. "Determination of complex refractive index of polystyrene microspheres from 370 to 1610 nm". In: *Physics in medicine and biology* 48 (Jan. 2004), pp. 4165–72. DOI: 10.1088/0031-9155/48/24/013.

[9]   Keir C. Neuman and Steven M. Block. "Optical trapping". In: *Review of Scientific Instruments* 75.9 (2004), pp. 2787–2809. DOI: 10.1063/1.1785844. eprint: https://doi.org/10.1063/1.1785844. URL: https://doi.org/10.1063/1.1785844.

[10] R S Dutra et al. "Polarization effects in optical tweezers". In: *Journal of Optics A: Pure and Applied Optics* 9.8 (July 2007), S221–S227. DOI: 10.1088/1464-4258/9/8/s15. URL: https://doi.org/10.1088/1464-4258/9/8/s15.

[11] Nathan Viana et al. "Towards absolute calibration of optical tweezers". In: *Physical review. E, Statistical, nonlinear, and soft matter physics* 75 (Mar. 2007), p. 021914. DOI: `10.1103/PhysRevE.75.021914`.

[12] Joost van Mameren. *Optical tweezers: where physics meets biology*. 2008. URL: `https://physicsworld.com/a/optical-tweezers-where-physics-meets-biology/`.

[13] Keir C Neuman and Attila Nagy. "Single-molecule force spectroscopy: optical tweezers, magnetic tweezers and atomic force microscopy". In: *Nature methods* 5.6 (June 2008), pp. 491–505. ISSN: 1548-7091. DOI: `10.1038/nmeth.1218`. URL: `https://europepmc.org/articles/PMC3397402`.

[14] Oliver Otto et al. "Optical tweezers with 2.5 kHz bandwidth video detection for single-colloid electrophoresis". In: *The Review of scientific instruments* 79 (Mar. 2008), p. 023710. DOI: `10.1063/1.2884147`.

[15] "High-resolution, long-term characterization of bacterial motility using optical tweezers". English (US). In: *Molecular Pharmaceutics* 6.11 (2009), pp. 831–835. ISSN: 1543-8384. DOI: `10.1038/nmeth.1380`.

[16] M. S. Rocha. "Optical tweezers for undergraduates: Theoretical analysis and experiments". In: *American Journal of Physics* 77.8 (2009), pp. 704–712. DOI: `10.1119/1.3138698`. eprint: `https://doi.org/10.1119/1.3138698`. URL: `https://doi.org/10.1119/1.3138698`.

[17] Arnau Farré and Mario Montes-Usategui. "A force detection technique for single-beam optical traps based on direct measurement of light momentum changes". In: *Opt. Express* 18.11 (May 2010), pp. 11955–11968. DOI: `10.1364/OE.18.011955`. URL: `http://www.opticsexpress.org/abstract.cfm?URI=oe-18-11-11955`.

[18] Jan Klaers et al. "Bose–Einstein condensation of photons in an optical microcavity". In: *Nature* 468.7323 (Nov. 2010), pp. 545–548. ISSN: 1476-4687. DOI: `10.1038/nature09567`. URL: `http://dx.doi.org/10.1038/nature09567`.

[19] Rafael Dutra et al. "Absolute calibration of optical tweezers including aberrations". In: *Applied Physics Letters* 100 (Mar. 2012). DOI: `10.1063/1.3699273`.

[20] Benjamin Landenberger et al. "Microfluidic sorting of arbitrary cells with dynamic optical tweezers". In: *Lab Chip* 12 (17 2012), pp. 3177–3183. DOI: `10.1039/C2LC21099A`. URL: `http://dx.doi.org/10.1039/C2LC21099A`.

[21] Richard W Bowman and Miles J Padgett. "Optical trapping and binding". In: *Reports on Progress in Physics* 76.2 (Jan. 2013), p. 026401. DOI: `10.1088/0034-4885/76/2/026401`. URL: `https://doi.org/10.1088/0034-4885/76/2/026401`.

[22] Ignacio Martínez et al. "A Simple Technique Based on a Single Optical Trap for the Determination of Bacterial Swimming Pattern". In: *PloS one* 8 (Apr. 2013), e61630. DOI: `10.1371/journal.pone.0061630`.

[23] Johann Berthelot et al. "Three-dimensional manipulation with scanning near-field optical nanotweezers". In: *Nature Nanotechnology* 9 (Mar. 2014), pp. 295–299. DOI: `10.1038/nnano.2014.24`.

[24]   X. Yan et al. "Stochastic Dynamic Trapping in Robotic Manipulation of Micro-Objects Using Optical Tweezers". In: *IEEE Transactions on Robotics* 32.3 (2016), pp. 499–512. DOI: `10.1109/TRO.2016.2539378`.

[25]   Arne Gennerich. *Optical Tweezers: Methods and Protocols*. Vol. 1486. Jan. 2017. ISBN: 978-1-4939-6419-2. DOI: `10.1007/978-1-4939-6421-5`.

[26]   Zhujing Xu and Tongcang Li. "Detecting Casimir torque with an optically levitated nanorod". In: *Phys. Rev. A* 96 (3 Aug. 2017), p. 033843. DOI: `10.1103/PhysRevA.96.033843`. URL: `https://link.aps.org/doi/10.1103/PhysRevA.96.033843`.

[27]   NobelPrize.org. *The Nobel Prize in Physics 2018*. 2018. URL: `https://www.nobelprize.org/prizes/physics/2018/summary/`.

[28]   Paolo Polimeno et al. "Optical tweezers and their applications". In: *Journal of Quantitative Spectroscopy and Radiative Transfer* 218 (2018), pp. 131–150. ISSN: 0022-4073. DOI: `https://doi.org/10.1016/j.jqsrt.2018.07.013`. URL: `http://www.sciencedirect.com/science/article/pii/S002240731830445X`.

[29]   Bin Liu et al. "Holding and transferring matter-wave solitons against gravity by spin–orbit-coupling tweezers". In: *New Journal of Physics* 22.4 (Apr. 2020), p. 043004. ISSN: 1367-2630. DOI: `10.1088/1367-2630/ab7cb1`. URL: `http://dx.doi.org/10.1088/1367-2630/ab7cb1`.

[30]   O. Contreras-Vergara et al. "Harmonic oscillator Brownian motion: Langevin approach revisited". In: *Revista Mexicana de Física E* 18 (Jan. 2021), p. 97. DOI: `10.31349/RevMexFisE.18.97`.